Title	Coastal iodine emissions: part 2. Chamber experiments of particle formation from Laminaria digitata-derived and laboratory-generated I2
Author(s)	Monahan, Ciaran; Ashu-Ayem, Enowmbi R.; Nitschke, Udo; Darby, Steven B.; Smith, Paul D.; Stengel, Dagmar B.; Venables, Dean S.; O'Dowd, Colin D.
Publication date	2012
Original citation	MONAHAN, C., ASHU-AYEM, E. R., NITSCHKE, U., DARBY, S. B., SMITH, P. D., STENGEL, D. B., VENABLES, D. S. & O'DOWD, C. D. 2012. Coastal Iodine Emissions: Part 2. Chamber Experiments of Particle Formation from Laminaria digitata-Derived and Laboratory-Generated I2. Environmental Science & Technology, 46, 10422-10428. doi: 10.1021/es3011805
Type of publication	Article (peer-reviewed)
Link to publisher's version	http://dx.doi.org/10.1021/es3011805 Access to the full text of the published version may require a subscription.
Rights	**Copyright © 2012 American Chemical Society. This document is the Accepted Manuscript version of a Published Work that appeared in final form in Environmental Science and Technology, copyright © American Chemical Society after peer review and technical editing by the publisher. To access the final edited and published work see http://pubs.acs.org/doi/abs/10.1021/es3011805**
Item downloaded from	http://hdl.handle.net/10468/788

Coastal Iodine Emissions: Part 2. Chamber Experiments into Particle Formation from Laminaria digitata-Derived and Laboratory-Generated I2

Journal:	*Environmental Science & Technology*
Manuscript ID:	Draft
Manuscript Type:	Article
Date Submitted by the Author:	n/a
Complete List of Authors:	monahan, ciaran; NUIG, Physics Ashu-Ayem, Tina; UCC, Chemistry Nitschke, Udo; NUIG, SoNS Derby, Steven; UCC, Chemistry Smith, Paul; UCC, Chemistry Stengal, Dagmar; NUIG, SoNS Venables, Dean; University of College Cork, Chemistry o'Dowd, Colin; NUIG, Physics

Coastal Iodine Emissions: Part 2. Chamber Experiments into Particle Formation from *Laminaria digitata*-Derived and Laboratory-Generated I_2

CIARAN MONAHAN[1],, ENOWMBI R. ASHU-AYEM[2], UDO NITSCHKE[3], STEVEN B. DARBY[2], PAUL D. SMITH[2], DAGMAR B. STENGEL[3], DEAN S. VENABLES[2] AND COLIN D. O'DOWD[1]*

[1]School of Physics and Centre for Climate & Air Pollution Studies, Ryan Institute, National University of Ireland Galway, Galway, Ireland, [2]Department of Chemistry and Environmental Research Institute, University College Cork, Cork, Ireland, and [3]Botany and Plant Science, School of Natural Sciences and Ryan Institute, National University of Ireland Galway, Galway, Ireland

Received 2012, Revised manuscript received 2012. Accepted, 2012

Laboratory studies into particle formation from *L. digitata* macroalgae were undertaken to elucidate aerosol formation for a range of I_2 (0.3-76 ppb$_v$) and O_3 (<3-96 ppb$_v$) mixing ratios and light-levels (E_{PAR} = 15-235 µmol photons m^{-2} s^{-1}). No clear pattern was observed for I_2 or aerosol parameters as a function of light-levels; however, aerosol mass fluxes (assuming I_2O_4 gas-to-particle conversion) and particle number concentrations were correlated (R^2=0.7 and 0.95, respectively) with I_2 mixing ratios for low O_3 mixing ratios (<3 ppb$_v$). Additional experiments into particle production as a function of laboratory-generated I_2, over a mixing ratio range of 1-8 ppb$_v$, were conducted under moderate O_3 mixing ratios (~24 ppb$_v$) where a clear, 100-fold or greater, increase in the aerosol number concentrations and mass fluxes was observed compared to the low-O_3 experiments. A linear relationship between particle concentration and I_2 was found, in reasonable agreement with previous studies. Scaling the laboratory relationship to aerosol concentrations typical of the coastal boundary layer suggests a I_2 mixing ratio range of 6-93 ppt$_v$ can account for the observed particle production events. Aerosol number concentration produced from I_2 is more than a factor of 10 higher than that produced from CH_2I_2 for the same mixing ratios.

Introduction

The release of volatile iodine organic compounds and of molecular iodine (I_2) into the marine boundary layer (MBL) has been linked to the rapid production of large numbers of new, ultrafine, aerosol particles [1-4]. The nucleation and growth events have been observed to occur most frequently in coastal areas under conditions of solar irradiation and low tide. Initial studies on the dominant aerosol precursor focused on the release of CH_2I_2 by shore biota [2, 5, 6]; however, it was later shown that the dominant iodine source is more likely to be I_2 [7, 8]. In fact, *McFiggans.* (2004) [7] found that the iodine flux from I_2 was three orders of magnitude higher than that from CH_2I_2, due to a higher photolysis rate for I_2 . Photo-chemically produced iodine atoms react rapidly with ozone to produce iodine monoxide radicals (IO) which subsequently self-react to form iodine dioxide radicals (OIO) and I_2O_4. A fraction of the newly formed I_2O_4 may then form new particles while reaction with IO may form I_2O_3 which again may react with O_3 to form I_2O_5 [7, 9-11]. Modelling studies have also suggested that OIO or I_xO_y molecules may co-nucleate or co-condense with other molecules such as H_2SO_4 and/or low-volatility organic compounds [12, 13]. Most previous laboratory studies have focused on the common kelp *Laminaria (L.) digitata* which is prone to high I_2 emission rates when exposed to oxidative stresses[14,15,16, 17,18,19]. Field-chamber experiments (using scrubbed marine air) have shown a linear correlation between new particle formation and I_2 mixing ratios from *Laminaria* and *Fucus* species [20] in the vicinity of Mace Head, located on the Irish – Atlantic coastline [21]. This work extends previous studies[22,23,24] into particle production from I_2 emissions from a number of different seaweed species in that it specifically focuses on aerosol formation for a wide range of I_2 mixing ratios from a strong I_2 emitter, *L. digitata,* under a wider range of conditions (i.e. various light levels and ozone mixing ratios), followed by the quantification of aerosol production from laboratory-generated I_2, for moderate ozone mixing ratios.

This report comprises Part 2 of a two-part study – Part 1 focuses on I_2 emission rates from *L. digitata* under various environmental conditions and is reported in *Ashu-Ayem et al.,* (2012).

Experimental Section

Experiments were carried out in an atmosphere simulation chamber comprising a cylindrical FEP bag housed inside a 2 m long enclosure. The chamber volume was 2.2 m^3 and its surface area was approximately 10 m^2. A photolysis light source, comprising an externally-mounted 2 kW xenon lamp (Rige Lighting), produced a circular collimated beam above the chamber. The lamp spectrum (400 to 850 nm, λ_{max} = 550 nm) provided simulated Photosynthetically Active Radiation (PAR) spectrum leading to an I_2 chamber photolysis rate of 0.0075 ± 0.0010 s^{-1}. Ozone was added using an Ozone Lab model OL80W/FM ozone generator. An incoherent broadband cavity-enhanced absorption spectroscopy (IBBCEAS) system was the principle tool for analyzing the gas phase composition of the chamber[26,27]. The IBBCEAS comprised two optical cavities across the length of the chamber: a blue channel (420 to 460 nm) for IO and a green channel (520 to 560 nm) for I_2 and OIO. Reference spectra for IO and OIO were obtained from *Spietz et al.* and *Bloss et al.* respectively, and convoluted to this particular instrument function[28,29]. O_3 was monitored using a UV absorption monitor (2B Technologies model 202) with a sampling rate of 1 L min^{-1}.

A nano scanning mobility particle sizer (n-SMPS), comprising a Thermo Systems Inc. (TSI) model 3776 condensation particle counter with a TSI model 3085 differential mobility analyzer, was operated continuously to measure particle sizes from 3nm to 20nm while a TSI model 3034 scanning mobility particle sizer (SMPS) was used in conjunction with the n-SMPS to measure particle size ranges a further 20 nm – 500 nm. The SMPS was only available for the third set of experiments. The n-SMPS and SMPS were operated with a time resolution of 20 s and 120 s respectively.

Repeated measurements in the chamber in the absence of *L. digitata* showed zero or close to zero particles, zero I_2, and levels of O_3 around the detection level of the instrument. Two types of static experiments were conduced on *L. digitata*: (1) iodine emission and subsequent particle formation from five replicas were examined under “low” (15 μmol photons m^{-2} s^{-1}), “medium” (100 μmol photons m^{-2} s^{-1}) and “high” (235 μmol photons m^{-2} s^{-1}) irradiances and under very ozone mixing ratios (< 3 ppb_v); and (2) iodine emissions and particle formation under low (15 μmol photons m^{-2} s^{-1}) irradiances but with ozone mixing ratios of the order of ~94 ppb_v. It should be noted that “high” light conditions here corresponds to 15% of the upper light limit that algae would be exposed to under real-world conditions. A third set of experiments were conducted on a range of mixing ratios of laboratory-generated I_2 under flow-through conditions and ozone mixing ratios ~24 ppb_v. For the *L. digitata* experiments, algae were placed in a 33 L tray filled with natural seawater which and were allowed to acclimatise over 10 minutes afterwhich the seawater was gradually drained over the following 10 minutes (i.e. to mimic an outgoing tide). A complete description of experimental methodologies can be found in *Ashu-Ayem et al.,* (2012)

Results & Discussion

Particle Formation Under Different Light Conditions and Low O_3. *L. digitata* samples were exposed to irradiances of E_{PAR}= 15, 100 and 235 µmol photons m^{-2} s^{-1}, labelled “low”, “medium” and “high” light conditions, respectively under static-chamber flow conditions. Experiments were performed at each light-level using five replicate *L. digitata* specimens to account for potential high variability in I_2 emission rates as previously observed[23] (See Table 1 in *Ashu-Ayem et al.*, (2012), and Supplementary Information for full experimental summary).

Particle formation was observed in all experiments when exposed to light and low-O_3 air. A characteristic strong particle burst, ~10-30 s after the start of the experiment, and peaking at concentrations ranging from 2.6 $\times 10^4$ cm^{-3} - 3.9 $\times 10^7$ cm^{-3}, corresponding to a range I_2 mixing ratios from 5.3 – 76.3 ppb_v, was observed. Figure 1 illustrates the evolution of the aerosol size distribution, O_3, I_2, and IO mixing ratios, the aerosol condensation mass flux (determined by the increase in nSMPS-derived volume, taking an I_2O_4 density of 2.5 g cm^{-3}), and number concentration. For medium light levels, I_2 mixing ratios of 1.1 - 20.2 ppb_v led to particle concentrations of 7 $\times 10^3$ cm^{-3} - 3.9 $\times 10^6$ cm^{-3}, while for high light levels, particle concentration ranged from 2.1 $\times 10^6$ cm^{-3} - 3.8 $\times 10^7$ cm^{-3} for I_2 mixing ratios of 4.1-36.8 ppb_v. The condensable mass flux for the low, medium and high light-level experiments ranged from 2.4 $\times 10^{-10}$ µg cm^{-3} s^{-1} – 1.7 $\times 10^{-7}$ µg cm^{-3} s^{-1}, 2.3 $\times 10^{-10}$ µg cm^{-3} s^{-1} - 1.7 $\times 10^{-8}$ µg cm^{-3} s^{-1} and 2.5 $\times 10^{-9}$ µg cm^{-3} s^{-1} - 5.3 $\times 10^{-7}$ µg cm^{-3} s^{-1}, respectively. Full details are tabulated in Table S1 in Supplementary Material.

The experiments in this study did not reveal and clear pattern between biomass, light-levels and either I_2 mixing ratios (as discussed in Part 1 of the study) or particle concentration. However, for the low and medium light-level experiments, a high correlation coefficient, fitted in log—log space, was found between mass flux and I_2 mixing ratio (R^2=0.7 and 0.95,respectively). Similarly high correlations were found for number concentration and I_2 mixing ratio (R^2=0.83 for low light-levels and 0.98 for medium light-levels). For the highest light-level, R^2 for mass flux as a function of I_2 mixing ratio was -0.02, in stark contrast to the low and medium light levels. From the 5 high light-level replicates, two concurrent samples (#12 and #13) stand out in that they are associated with relatively high biomass, quite low I_2 mixing ratios, and the highest mass flux. Variability in I_2 emissions could explain the low I_2 mixing ratios resulting from moderate to high amounts of biomass; however, the aerosol condensation flux yield for the corresponding I_2 mixing ratios is 1-2 orders of magnitude higher in these samples compared to all others (specifically, the ratio of mass flux over I_2 mixing ratio for these two samples ranges from 2-8 x 10^{-8} µg cm^{-3} s^{-1} ppb_v^{-1} while the ratio for the other samples ranges from 4 x 10^{-11} to 5 x 10^{-9} µg cm^{-3} s^{-1} ppb_v^{-1}). Such ratios are equivalent to those observed in the later O_3 – rich experiments.

It should be noted that the air in the chamber prior to each replicate had an O_3 mixing ratio that was at or below detection limit of 3 ppb_v; however, particle formation still proceeded. Therefore, O_3 was present in sufficient concentrations to produce significant quantities of aerosol, although still at or below detection limits. It is thought that either O_3 was produced by trace amounts of VOCs and NOx entering the chamber from laboratory air or direct entrainment of O_3 from laboratory air. We suggest that samples #12 and # 13 were potentially influenced by slightly elevated O_3 mixing ratios resulting in significant increases in aerosol yield, thus also explaining the low I_2 mixing ratios for relatively high biomass abundance. In fact, peak O_3 values recorded above the detection limit were 3-4 times higher for these two particular cases compared to the other samples (even spiking at 18 ppb_v). In light of the suspicion relating to comparability of the replicate #12 and #13 experiments in terms of O_3 upper mixing ratios, we have removed these cases from further analysis. The remaining three data lead to a R^2=0.98 for a log-log fit, indicating minimal scatter across these remaining samples. The remaining low, medium and high light-level datasets were grouped together, excluding sample #12 and #13, for an overall analysis and the inter-relationships between mass flux and concentration, as a function of mixing ratio, are shown in Figure 2. The mass flux versus I_2 mixing ratio exhibited a correlation of R^2=0.72, while the number concentration exhibited a correlation of R^2=88 with mixing ratio. Further investigations are required to address the variability in I_2 emission rates from *L. digitata*, as discussed in more detail in Part 1, *Ashu-Ayem et al.,* (2012).

Particle Formation Under Low Light Conditions and High O_3. An experiment composed of five replicates (replicates #21 - #25 - See Table 2 in Part 1) was also carried out. All algal specimens were of similar age and weight as those in the low light - low O_3 experiment (see Table S.1) Experimental conditions were kept the same as those of replicates #16 - #20 (i.e. low light) except for O_3 mixing ratios of 92-96 ppb_v. As in the previous experiments under low O_3, mixing ratios, the resulting I_2 mixing ratio varied enormously from sample to sample with no correlation between biomass being observed. This, in turn, led to variability in the characteristics of the resultant aerosol number concentration and mass flux. For the general collection of replicates, a higher rate of aerosol mass flux was observed under high O_3 conditions, perhaps resulting from a combined O_3 influence on both increased I_2 emissions resulting from potential oxidative stress of the algae along with increased particle production through oxidation processes; however, it is not possible to distinguish between the two processes since oxidative stress was not quantified in this experimental set up.

A typical particle size distribution evolution associated with this experiment is shown in Figure 3 where the experiment was observed to yield concentrations of particles of 3.5×10^7 cm^{-3} associated with I_2 mixing ratios of 17 ppb$_v$. In each of the replicates, an initial peak was observed followed by a second and stronger peak shortly after a steep rise in I_2 and IO mixing ratios. This can be seen in Figure 3, where the initial, and less intense peak was observed at ~11:40 am and the subsequent, stronger, peak was seen at ~12:10 pm. The maximum particle number concentration occurs at 4.2×10^7 cm^{-3}; however, the true concentration is expected to be higher as the growth rate of newly formed particles is so rapid that the mode diameter rapidly grows past the upper diameter detection limit of the nSMPS.

The overall particle number concentration increased from between 1×10^4 cm^{-3} and 1×10^7 cm^{-3} during the low ozone mixing ratio experiment to greater than 1×10^7 cm^{-3} during the high O_3 mixing ratio experiment, although due to the rapid modal growth out of the measurement size range, no quantitative relationship can be derived. The mass flux ranged from 8.2×10^{-8} µg cm^{-3} s^{-1} to 1.2×10^{-6} µg cm^{-3} s^{-1} , compared to 2.3×10^{-10} µg cm^{-3} s^{-1} to 1.7×10^{-7} µg cm^{-3} s^{-1} for a the low O_3, low light experiment.

This indicates at least 2 orders of magnitude more aerosol mass production in the presence of abundant ozone mixing ratios.

The effects of exposure of *L. digitata* to O_3 and the subsequent enhancement in the particle number concentration by several orders of magnitude have been reported in previous studies [9, 15, 17]; however, what remains unclear in these experiments is if exposure to O_3 leads to an increased I_2 net production rates ($P > 0.05$; see Table 1 and 2 in Part 1) in experiments with higher O_3 mixing despite the specimens being in similar light conditions (15 μmol photons m^{-2} s^{-1}), although there is a trend of higher net production rates if normalised to biomass weight. For this set of experiments, there was no conclusive statistical link between particle number concentration and I_2 mixing ratios; however, particle concentrations were generally higher for the high ozone mixing ratios. The lack of a statistical link, as suggested above, may be due to the rapid growth of the nucleation mode out of the nSMPS detection range.

IO trends tracked generally that of I_2, however, mixing ratios were typically two orders of magnitude lower. OIO, a by-product of the IO-IO self-reaction, is not detected despite having being considered the main precursor of iodine oxide aerosol particles. The interactions between I_2, IO and OIO are discussed in Part 1 of the study where the lack of detectable OIO (detection limit 30 ppt_v) is attributed to fast reactions between OIO and I atoms under the mixing ratio conditions in the chamber.

Particle Production as a Function of I_2 Mixing Ratio. In order to further study the role of I_2 in particle formation, a set of experiments were conducted under laboratory generated and controlled I_2 mixing ratios and a moderate O_3 mixing ratio of 24 ppb_v, regarded as representative of tropospheric conditions [30]. The experiments were carried out with a "flow through" configuration of 225 L min^{-1} applied to the chamber where light intensity was fixed at 100 µmol photons m^{-2} s^{-1} and I_2 mixing ratios varied from 1 ppb$_v$ to 8 ppb$_v$ (see Table 1). The flow-through experiment did not comprise continuous supply of O_3 and I_2, more so, O_3 concentrations were set to 24 ppb$_v$ in the chamber and then a pulse of I_2 was introduced. Controlled I_2 mixing ratios were generated by evaporating I_2-methanol solutions of known concentrations to dryness, followed by heating the I_2 residue in a stream of nitrogen into the chamber.

In each experiment, on mixing I_2 and O_3 in the photolysis chamber, both mixing ratios were rapidly reduced due to combined photolysis, oxidation and subsequent formation and growth of the aerosol. For each replicate the total particle number concentration increased rapidly initially, reaching its peak after about 10 minutes from the inception of photolysis and then rapidly decayed. Figure 4 illustrates the general evolution of the aerosol number concentrations in relation to the gas species mixing ratios over time. For the example shown in Figure 4, the initial ozone mixing ratio was 24 ppb$_v$, and after the introduction of I_2 into the chamber, I_2 peaked at 6.6 ppb$_v$ while simultaneously IO peaked at 0.1 ppb$_v$. tens of seconds later, particle production was observed and after about five minutes, a peak concentration of 9 x 10^7 cm^{-3} was observed. By the time the peak aerosol concentration was observed, both I_2 and IO mixing ratios had reduced by a factor of 2. I_2 decayed more rapidly than IO. For the other experiments, I_2 ranged from 1.0 ppb$_v$ to 8.1 ppb$_v$ and the total aerosol concentration ranged from 2.5×10^6 cm^{-3} to 1.1×10^8 cm^{-3}, respectively, while 3 nm particle concentration ranged from 8.9×10^4 cm^{-3} to 3.7×10^6 cm^{-3}, respectively.

Comparison of the condensing mass flux and number concentration, over the range of I_2 mixing ratios overlapping (i.e. 1-8 ppb$_v$) in the low ozone experiment and the moderate ozone experiment, illustrates generally 2-3 orders of magnitude greater mass flux in the moderate ozone experiment (see Figure 5).

The total particle number concentration, as well as the 3 nm particle concentration increased linearly as the initial I_2 mixing ratio was increased. The linear fit (in linear space) between I_2 and total particle concentration is shown in Figure 4 and was found to be N_{tot} $(cm^{-3}) = 1.34 \times 10^7$ I_2 (ppb_v) while the linear fit between 3 nm particle concentration and I_2 was found to be N_{3nm} $(cm^{-3}) = 4.69 \times 10^5$ I_2 (ppb_v). The total particle concentration as a function of IO was also seen to increase linearly with increasing IO.

The correlations between I_2 and particle concentrations, shown in Figure 6, were $R^2=0.7$ for both the total and 3 nm particle concentrations, with more scatter having been observed for lower values of I_2. During the course of the present study, other species such as HOI may have been preferentially formed at different mixing ratios but not detectable by IBBCEAS methods and may contribute a "missing" component in the cycle. The relationship between particle concentration and I_2 in this study is compared to that from *Sellegri et al.,* (2005), extending up to 400 ppt_v, along with the relationship between particle concentration and CH_2I_2 mixing ratios reported by *Burkholder et al.,* (2004) and *Jimenez et al.*, (2003). While the I_2 mixing ratios in this study are higher than *Sellegri et al.* comparison of both relationships indicates a greater particle concentration generated by *Sellegri et al.* at low I_2 mixing ratios, but relatively similar concentrations at high I_2 mixing ratios. Both this study and that of *Sellegri et al.* illustrate at least an order of magnitude higher aerosol yield from I_2 compared to that from CH_2I_2, consistent with differences in photolysis lifetimes.

Comparison to Ambient Measurements. Results arising from the flow-through chamber studies reported here can be directly compared to field measurements of coastal, iodine-driven, new particle production events [2, 31]. While the concentrations in the laboratory are significantly higher than observed in the field, they can be extrapolated down to lower concentrations in order to estimate the I_2 mixing ratios required to produce observed particles in coastal events such as those at Mace Head. Over the period from 1st May 2010 to the 1st August 2010, 28 typical clean air coastal production events were analysed and were found to have a total particle concentration range between 7.8×10^4 cm^{-3} - 1.2×10^6 cm^{-3} and a peak 3 nm particle concentration range of 4.3×10^3 cm^{-3} - 9.4×10^4 cm^{-3}. Scaling the relationships between particle concentration and I_2 downward to observed concentrations in the field points to a coastal boundary layer I_2 mixing ratio of 6-93 ppt_v. Values in this range are in line with a previous studies by *Saiz-Lopez and Plane* (2004) who found that the nucleation events observed at Mace Head ($N_{3nm} = 5\times10^4$ cm^{-3}) could be produced by the daytime photolysis of 10 ppt_v I_2, typical of the daytime mixing ratios observed at low tide during the measurement period.

ACKNOWLEDGMENT

We thank Science Foundation Ireland for supporting this research through grants 07/RFP/GEOF716 and 09/RFP/CAP2509. UN gratefully appreciates financial support through the Irish Research Council for Science, Engineering and Technology (IRCSET "Embark Initiative"). COD and CM also acknowledge EC funding under the MAP and EUCAARI and EUSAAR.

References

1. McFiggans, G.; Bale, C. S. E.; Ball, S. M.; Beames, J. M.; Bloss, W. J.; Carpenter, L. J.; Dorsey, J.; Dunk, R.; Flynn, M. J.; Furneaux, K. L.; Gallagher, M. W.; Heard, D. E.; Hollingsworth, A. M.; Hornsby, K.; Ingham, T.; Jones, C. E.; Jones, R. L.; Kramer, L. J.; Langridge, J. M.; Leblanc, C.; LeCrane, J. P.; Lee, J. D.; Leigh, R. J.; Longley, I.; Mahajan, A. S.; Monks, P. S.; Oetjen, H.; Orr-Ewing, A. J.; Plane, J. M. C.; Potin, P.; Shillings, A. J. L.; Thomas, F.; von Glasow, R.; Wada, R.; Whalley, L. K.; Whitehead, J. D., Iodine-mediated coastal particle formation: an overview of the Reactive Halogens in the Marine Boundary Layer (RHaMBLe) Roscoff coastal study. *Atmos. Chem. Phys.* **2010,** 10, (6), 2975-2999.
2. O'Dowd, C. D.; Jimenez, J. L.; Bahreini, R.; Flagan, R. C.; Seinfeld, J. H.; Hameri, K.; Pirjola, L.; Kulmala, M.; Jennings, S. G.; Hoffmann, T., Marine aerosol formation from biogenic iodine emissions. *Nature* **2002,** 417, (6889), 632-636.
3. Saiz-Lopez, A.; Shillito, J. A.; Coe, H.; Plane, J. M. C., Measurements and modelling of I2, IO, OIO, BrO and NO3 in the mid-latitude marine boundary layer. *Atmos. Chem. Phys.* **2006,** 6, (6), 1513-1528.
4. Whitehead, J. D.; McFiggans, G. B.; Gallagher, M. W.; Flynn, M. J., Direct linkage between tidally driven coastal ozone deposition fluxes, particle emission fluxes, and subsequent CCN formation. *Geophys. Res. Lett.* **2009,** 36, (4), L04806.
5. Hoffmann, T.; O'Dowd, C. D.; Seinfeld, J. H., Iodine oxide homogeneous nucleation: An explanation for coastal new particle production. *Geophys. Res. Lett.* **2001,** 28, (10), 1949-1952.
6. Jimenez, J. L.; Bahreini, R.; Cocker, D. R., III; Zhuang, H.; Varutbangkul, V.; Flagan, R. C.; Seinfeld, J. H.; O'Dowd, C. D.; Hoffmann, T., New particle formation from photooxidation of diiodomethane (CH2I2). *J. Geophys. Res.* **2003,** 108, (D10), 4318.
7. McFiggans, G.; Coe, H.; Burgess, R.; Allan, J.; Cubison, M.; Rami Alfarra, M.; Saunders, R.; Saiz-Lopez, A.; Plane, J. M. C.; Wevill, D.; Carpenter, L.; Rickard, A. R.; Monks, P. S., Direct evidence for coastal iodine particles from Laminaria macroalgae; linkage to emissions of molecular iodine. *Atmos. Chem. Phys. Discuss.* **2004,** 4, (1), 939-967.
8. Saiz-Lopez, A.; Plane, J. M. C., Novel iodine chemistry in the marine boundary layer. *Geophys. Res. Lett.* **2004,** 31, (4), L04112.
9. Burkholder, J. B.; Curtius, J.; Ravishankara, A. R.; Lovejoy, E. R., Laboratory studies of the homogeneous nucleation of iodine oxides. *Atmos. Chem. Phys.* **2004,** 4, (1), 19-34.
10. Kaltsoyannis, N.; Plane, J. M. C., Quantum chemical calculations on a selection of iodine-containing species (IO, OIO, INO3, (IO)2, I2O3, I2O4 and I2O5) of importance in the atmosphere. *Physical Chemistry Chemical Physics* **2008,** 10, (13), 1723-1733.
11. Pirjola, L.; O'Dowd, C.; Yoon, Y. J.; Sellegri, K., Modelling Iodine Particle Formation and Growth from Seaweed in a Chamber. *Environmental Chemistry* **2005,** 2, (4), 271-281.
12. Ciaran Monahan, Henri Vuollekoski , Markku Kulmala, and Colin O'Dowd, “Simulating Marine New Particle Formation and Growth Using the M7 Modal Aerosol Dynamics Modal,” *Advances in Meteorology*, vol. 2010, Article ID 689763, 9 pages, **2010**.

13. Vuollekoski, H.; Kerminen, V. M.; Anttila, T.; Sihto, S. L.; Vana, M.; Ehn, M.; Korhonen, H.; McFiggans, G.; O'Dowd, C. D.; Kulmala, M., Iodine dioxide nucleation simulations in coastal and remote marine environments. *J. Geophys. Res.* **2009,** 114, (D2), D02206.

14. Kupper, F. C.; Carpenter, L. J.; Gordon, B. M.; Palmer, C. J.; Waite, T. J.; Boneberg, E.-M.; Woitsch, S.; Weiller, M.; Abela, R.; Grolimund, D.; Potin, P.; Alison, B.; Luther, G. W., III; Kroneck, P. M. H.; Meyer-Klaucke, W.; Feitersm, M. C., Iodide Accumulation Provides Kelp with an Inorganic Antioxidant Impacting Atmospheric Chemistry. *Proceedings of the National Academy of Sciences of the United States of America* **2008,** 105, (19), 6954-6958.

15. Palmer, C. J.; Anders, T. L.; Carpenter, L. J.; KÃ¼pper, F. C.; McFiggans, G. B., Iodine and Halocarbon Response of Laminaria digitata to Oxidative Stress and Links to Atmospheric New Particle Production. *Environmental Chemistry* **2005,** 2, (4), 282-290.

16. Bale, C.; Ingham, T.; Commane, R.; Heard, D.; Bloss, W., Novel measurements of atmospheric iodine species by resonance fluorescence. *Journal of Atmospheric Chemistry* **2008,** 60, (1), 51-70.

17. Dixneuf, S.; Ruth, A. A.; Vaughan, S.; Varma, R. M.; Orphal, J., The time dependence of molecular iodine emission from Laminaria digitata. *Atmos. Chem. Phys.* **2009,** 9, (3), 823-829.

18. Nitschke, U.; Ruth, A.; Dixneuf, S.; Stengel, D., Molecular iodine net production rates and photosynthetic performance of different thallus parts of Laminaria digitata; (Phaeophyceae) during emersion. *Planta* **2011,** 233, (4), 737-748.

19. Kundel, M.; Thorenz, U.; Petersen, J.; Huang, R.-J.; Bings, N.; Hoffmann, T., Application of mass spectrometric techniques for the trace analysis of short-lived iodine-containing volatiles emitted by seaweed. *Analytical and Bioanalytical Chemistry* **2012,** 402, (10), 3345-3357.

20. Sellegri, K.; Yoon, Y. J.; Jennings, S. G.; Oâ€™Dowd, C. D.; Pirjola, L.; Cautenet, S.; Chen, H.; Hoffmann, T., Quantification of Coastal New Ultra-Fine Particles Formation from In situ and Chamber Measurements during the BIOFLUX Campaign. *Environmental Chemistry* **2005,** 2, (4), 260-270.

21 O'Connor, T.C., S.G. Jennings, and C.D. O'Dowd, Highlights from 50 years of Aerosol Measurements at Mace Head, *Atmos. Res.*, 90, 338–355, doi:10.1016/j.atmosres.2008.08.014, **2008**.

22. Ball, S. M.; Hollingsworth, A. M.; Humbles, J.; Leblanc, C.; Potin, P.; McFiggans, G., Spectroscopic studies of molecular iodine emitted into the gas phase by seaweed. *Atmos. Chem. Phys.* **2010,** 10, (13), 6237-6254.

23. Huang, R. J., Seitz, K., Neary, T., O'Dowd, C. D., Platt, U., Hoffmann T., Observations of high concentrations of I2 and IO in coastal air supporting iodine-oxide driven coastal new particle formation, *Geophys. Res. Lett*, **2010**, 37, L03803, doi:10.1029/2009GL041467.

24. Huang, R. J., Seitz, K., Buxmann, J., Hornsby, K. E., Carpenter, L. J., Platt, U., Hoffmann, T.: In situ measurements of molecular iodine in the marine boundary layer: the link to macroalgal species and the implications for O3, IO, OIO and NOx, *Atmospheric Chemistry and Physics*, **2010**, 10, 4823-4833.

25. Ashu-Ayem, E.R., U, Nitschke, C. Monahan, J. Chen, S.B. Darby, P.D. Smith, C.D. O'Dowd, D. B. Stengel, D.S. Venables. Coastal iodine emissions: Part

1. Release of I_2 by *Laminaria digitata* in chamber experiments, submitted, *Environ. Sci. Tech*., **2012**

26. Gherman, T.; Venables, D. S.; Vaughan, S.; Orphal, J.; Ruth, A. A. Incoherent broadband cavity-enhanced absorption spectroscopy in the near-ultraviolet: application to HONO and NO2. *Environ. Sci. Technol*. **2008**, 42, 890-895.
27. Chen, J.; Wenger, J. C.; Venables, D. S. Near-ultraviolet absorption cross sections of nitrophenols and their potential influence on tropospheric oxidation capacity. *J. Phys. Chem*. A **2011**, 115, 12235-12242.
28. Spietz, P.; Gómez-Martín, J. C.; Burrows, J. P. Spectroscopic studies of the I2/O3 photochemistry Part 2. Improved spectra of iodine oxides and analysis of the IO absorption spectrum. *Photochem. Photobiol*. A **2005**, 176, 50-67.
29. Bloss, W. J.; Rowley, D. M.; Cox, R. A.; Jones, R. L. Kinetics and products of the IO self-reaction. *J. Phys. Chem*. A **2001**, 105, 7840-7854.
30. Derwent, R. G.; Simmonds, P. G.; Manning, A. J.; Spain, T. G., Trends over a 20-year period from 1987 to 2007 in surface ozone at the atmospheric research station, Mace Head, Ireland. *Atmospheric Environment* **2007,** 41, (39), 9091-9098.
31. O'Dowd, C. D.; Geever, M.; Hill, M. K.; Smith, M. H.; Jennings, S. G., New particle formation: Nucleation rates and spatial scales in the clean marine coastal environment. *Geophys. Res. Lett.* **1998,** 25, (10), 1661-1664.

Experiment	I_2 (ppb$_v$)	Initial O_3 (ppb$_v$)	Max Number Concentration (cm^{-3})	Mass Flux (µg cm^{-3} s^{-1})	3 nm Max Number Concentration (cm^{-3})
CH6	1.04	24	2.54×10^{6}	2.55×10^{-8}	8.88×10^{4}
CH4	1.73	24	5.07×10^{6}	5.89×10^{-8}	1.77×10^{5}
CH3	2.88	24	8.66×10^{7}	1.13×10^{-6}	3.03×10^{6}
CH2	4.98	24	9.06×10^{7}	1.20×10^{-6}	3.17×10^{6}
CH1	6.6	24	6.75×10^{7}	8.75×10^{-7}	2.36×10^{6}
CH5	8.1	24	1.05×0^{8}	2.49×10^{-6}	3.67×10^{6}

Table 1 Summary of experiments preformed with mixing ratios of I_2 and O_3 in a 2200 Litre chamber with a purge flow of 225 L min^{-1}.

FIGURE 1. (Top) Typical particle size distribution evolution (Sample #19) over time for *L. Digitata* in chamber without flow-through for low light conditions. (Bottom) Particle concentration, mass flux, I_2 mixing ratio and O_3 mixnign ratio.

FIGURE 2. Condensation mass flux and particle concentration as a function of I_2 mixing ratio. Low, medium and high light-level data are colour coded.

FIGURE 3. (Top) Particle size distribution evolution for *L.digitata* (Replicate #25) in chamber without flow-through with low light conditions and an initial mixing ratio of 95.8 ppb_v of O_3. (Bottom) Particle concentration, mass flux and I_2, IO, I_2 and O_3 mixing ratios.

FIGURE 4. (Top) Aerosol size distribution evolution for laboratory-generated I_2 flow-through experiment CH1. (Bottom) Particle concentration, I_2, IO, and O_3 mixing ratios for flow-through experiment CH1.

FIGURE 5. (top) Mass flux and (bottom) particle concentration for low-O_3, static-flow, and moderate-O_3, flow-through, experiments.

FIGURE 6. Particle concentration as a function of I_2 and CH_2I_2 for this study and previous studies. The mixing ratio range associated with previous studies is shown by horizontal lines on top of graph.

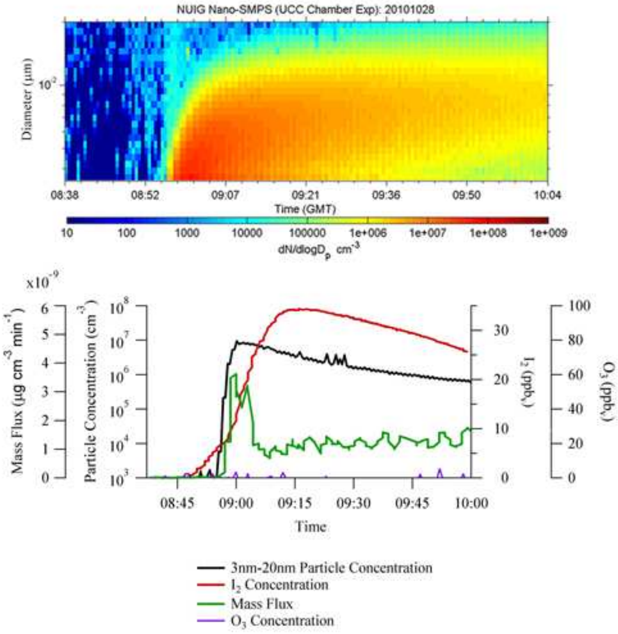

FIGURE 1. (Top) Typical particle size distribution evolution (Sample #19) over time for *L. Digitata* in chamber without flow-through for low light conditions. (Bottom) Particle concentration, mass flux, I_2 mixing ratio and O_3 mixnign ratio.

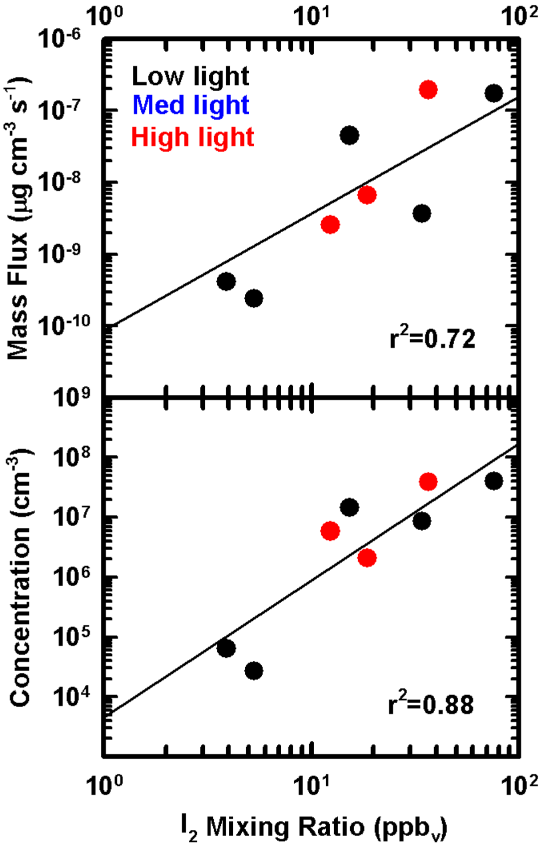

FIGURE 2. Condensation mass flux and particle concentration as a function of I_2 mixing ratio. Low, medium and high light-level data are colour coded.

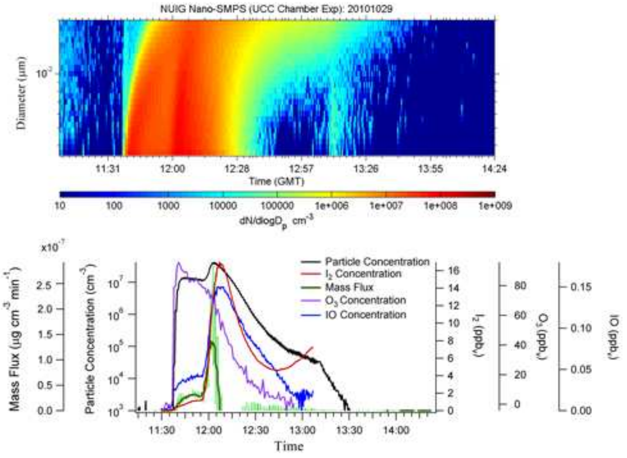

FIGURE 3. (Top) Particle size distribution evolution for *L.digitata* (Replicate #25) in chamber without flow-through with low light conditions and an initial mixing ratio of 95.8 ppb$_v$ of O_3. (Bottom) Particle concentration, mass flux and I_2, IO, I_2 and O_3 mixing ratios.

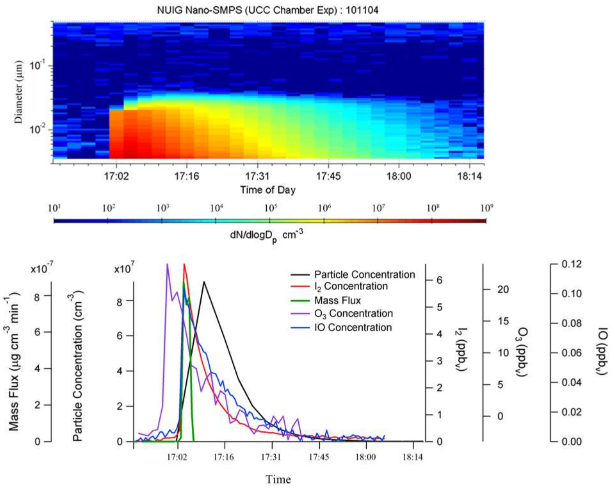

FIGURE 4. (Top) Aerosol size distribution evolution for laboratory-generated I_2 flow-through experiment CH1. (Bottom) Particle concentration, I_2, IO, and O_3 mixing ratios for flow-through experiment CH1.

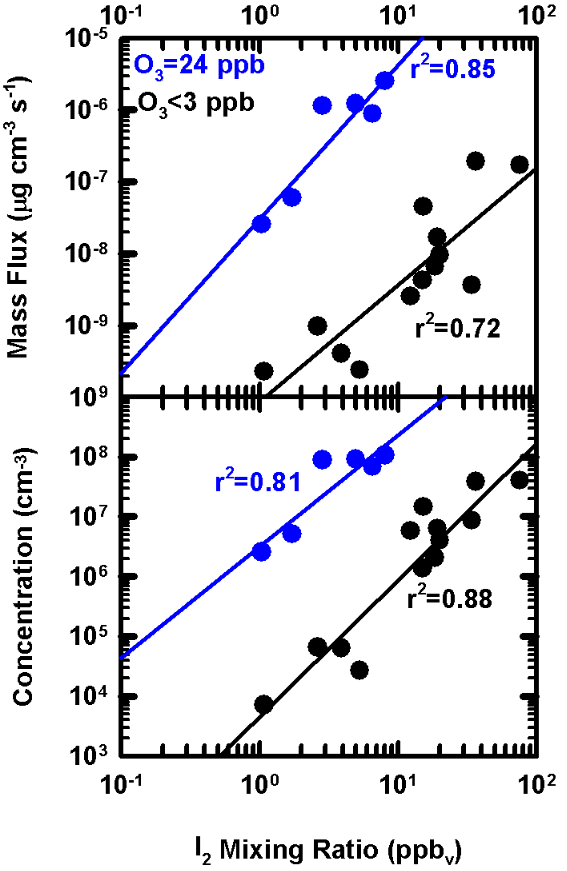

FIGURE 5. (top) Mass flux and (bottom) particle concentration for low-O_3, static-flow, and moderate-O_3, flow-through, experiments.

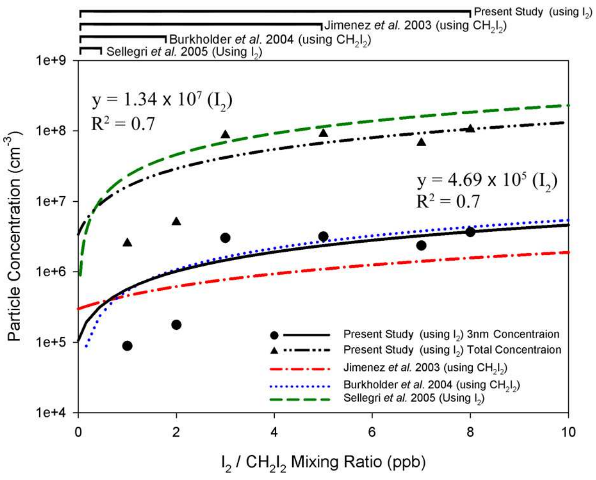

FIGURE 6. Particle concentration as a function of I_2 and CH_2I_2 for this study and previous studies. The mixing ratio range associated with previous studies is shown by horizontal lines on top of graph.

Supplementary Table S1. Laminaria Experiments Summary

Experiment Name	Maximum I_2 (ppb$_v$)	Max Particle Concentration (cm^{-3})	Fresh Weight (g)	Dry weight (g)	Max O_3 (ppb)	Maximum Mass Flux (μg cm^{-3} s^{-1})
With Added Ozone						
#21	0.29	7.9×10^{6}	274	54	94.6	7.2×10^{-7}
#22	4.23	1.9×10^{7}	175	35	93.4	8.2×10^{-8}
#23	30.92	2.9×10^{7}	213	48	95.6	2.0×10^{-7}
#24	23.77	4.2×10^{7}	185	44	91.5	1.2×10^{-6}
#25	16.96	3.5×10^{7}	171	35	95.8	2.9×10^{-7}
Low Light						
#16	5.34	2.6×10^{4}	355	79	-	2.4×10^{-10}
#17	3.92	6.3×10^{4}	238	46	-	4.1×10^{-10}
#18	15.39	1.4×10^{7}	229	54	-	4.4×10^{-8}
#19	34.29	8.5×10^{6}	676	155	-	3.6×10^{-9}
#20	76.33	3.9×10^{7}	185	50	-	1.7×10^{-7}
Med Light						
#6	15.22	1.4×10^{6}	311	48	-	4.2×10^{-9}
#7	20.21	3.9×10^{6}	380	66	-	9.5×10^{-9}
#8	19.46	6.3×10^{6}	272	41	-	1.7×10^{-8}
#9	1.09	7.0×10^{3}	253	42	-	2.3×10^{-10}
#10	2.65	6.5×10^{4}	03	50	-	9.7×10^{-10}
High Light						
#11	12.42	5.7×10^{6}	360	58	-	2.5×10^{-9}
#12	6.75	1.0×10^{7}	425	62	-	5.3×10^{-7}
#13	4.05	2.1×10^{7}	306	44	-	7.2×10^{-8}
#14	18.68	2.1×10^{6}	330	55	-	6.5×10^{-9}
#15	36.82	3.8×10^{7}	335	51	-	1.9×10^{-7}